ACS OMEGA

http://pubs.acs.org/journal/acsodf

Article

Enhanced Formaldehyde Oxidation Performance of the Mesoporous TiO_2(B)-Supported Pt Catalyst: The Role of Hydroxyls

Tongtong Wei, Xuejuan Zhao, Long Li, Lei Wang, Shenjie Lv, Lei Gao, Gaosong Yuan, and Licheng Li*

Cite This: *ACS Omega* 2022, 7, 25491−25501

Read Online

ACCESS | Metrics & More | Article Recommendations | Supporting Information

ABSTRACT: As one of the crystal phases of titania, TiO_2(B) was first utilized as a catalyst carrier for the oxidation of formaldehyde (HCHO). The mesoporous TiO_2(B) loaded with Pt nanoparticles enhanced the HCHO oxidation reaction whose reaction rate was 4.5−8.4 times those of other crystalline TiO_2-supported Pt catalysts. Simultaneously, Pt/TiO_2(B) exhibited long-term stable HCHO oxidation performance. The structural characterization results showed that in comparison with Pt/anatase, Pt/TiO_2(B) had more abundant hydroxyls, facilitating increasing the content of oxygen species. Studies on the role of hydroxyls in HCHO oxidation of Pt/TiO_2(B) illustrated that synergistic involvement of terminally bound hydroxyls and bridging hydroxyls in HCHO oxidation accelerated the transformation from HCHO to formate via dioxymethylene. Moreover, hydroxyls could avoid the accumulation of excessive formate on Pt/TiO_2(B) and promote the rapid oxidation of CO. Accordingly, the hydroxyl groups could accelerate each substep of formaldehyde oxidation, which enabled Pt/TiO_2(B) to exhibit excellent formaldehyde oxidation performance.

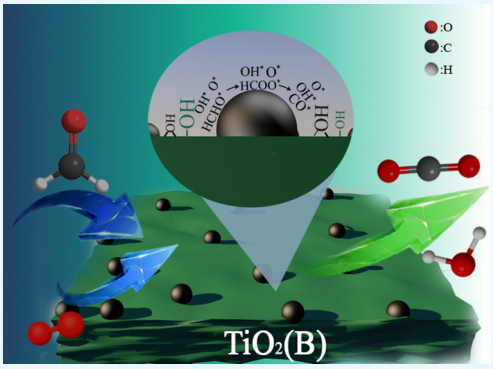

1. INTRODUCTION

Improvement in the lives of the masses arouses great public concern about the importance of health. Formaldehyde (HCHO) is considered as one of the most representative pollutants that can cause several diseases.[1,2] Among developed treatments, the oxidation of HCHO into nontoxic H_2O and CO_2 is an environmentally friendly and sustainable technology for HCHO removal.[3−5] To date, the supported noble metal catalysts have demonstrated more advanced catalytic performance compared with other types of HCHO oxidation catalysts. However, the high cost of noble metals severely limits the wide application of corresponding types of catalysts. Therefore, an attempt to promote the HCHO oxidation performance of catalysts is a feasible strategy for reducing the usage of noble metals.[6−8]

In the development course of catalysts, the regulation of the catalytic support is a relatively facile strategy to improve the catalytic performance of catalysts. TiO_2, Al_2O_3, CeO_2, activated carbon, cellulose triacetate, and so on were chosen as the support to investigate their HCHO oxidation performances.[9−12] It was found that the HCHO oxidation mechanisms on catalysts with various supports were distinct from each other. On this basis, several aforementioned materials were compounded together to give full play to their advantages.[13,14] Moreover, the approaches of enlarging specific areas, constructing hierarchical pores, and modifying surface properties have been proved to promote the dispersion of noble metals, adjust the electronic structure of active sites, accelerate the transfer of reactants, or enrich the hydroxyls of the support.[7,15−17] Although great progress has been made in the past, the strategy on the support regulation still attracts increasing attention for enhancing the HCHO oxidation performance of the catalyst.

TiO_2 is the most commonly used support in HCHO oxidation, which is usually regarded as the research benchmark in this area.[6,18,19] Anatase, rutile, and brookite are three crystal phases of TiO_2. Jiang et al. comparatively studied the turnover frequency (TOF) value for HCHO oxidation of the rutile TiO_2-supported Pt catalyst, which was five times as high as that of the anatase TiO_2-supported counterpart.[20] However, most research studies were carried out on anatase or anatase-rutile mixed phases because the anatase TiO_2 with a large surface area was easy to be synthesized. As for the brookite TiO_2, Yu et al. constructed hierarchical porous TiO_2-supported Pt catalysts. They found that the presence of a small amount of brookite TiO_2 in the support made negligible contribution to the HCHO oxidation performance of the catalyst.[21]

In addition to the aforementioned crystal phases, TiO_2(B) represents the metastable phase of TiO_2, which has the potential to be applied as a prospective lithium electrode,

Received: April 21, 2022
Accepted: July 4, 2022
Published: July 14, 2022

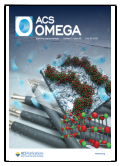

https://doi.org/10.1021/acsomega.2c02490
ACS Omega 2022, 7, 25491−25501

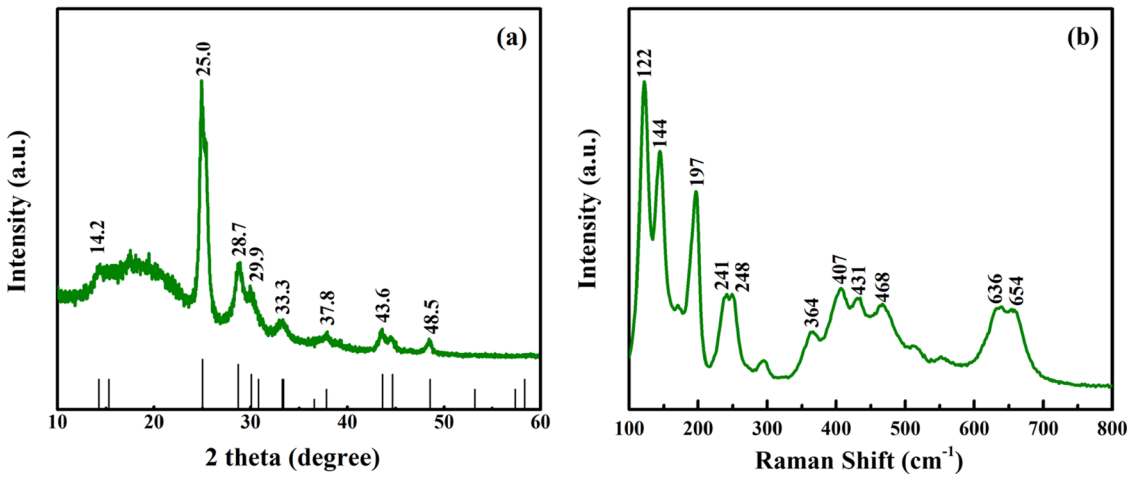

Figure 1. X-ray diffraction (XRD) pattern (a) and Raman spectrum (b) of Pt/TiO_2(B).

sensor material, and photocatalyst.[22−24] To the best of our knowledge, TiO_2(B) has not been used as a catalyst support for HCHO oxidation until now. Compared to the three aforementioned TiO_2 polymorphs in structure that have only one type of oxygen atom (i.e., three-coordinated one), TiO_2(B) features two, three, or four-coordinated oxygen atoms on the surface.[25−27] This leads to different surface properties between TiO_2(B) and other crystalline phases of titania. Previous research studies have demonstrated that the adsorbed water molecules could readily dissociate into hydroxyls on the TiO_2(B) surface.[25] It is well acknowledged that hydroxyl groups play a crucial role in the oxidation of HCHO by supported noble metal catalysts, such as promoting the adsorption and transfer of oxygen, assisting the catalyst in adsorbing HCHO, directly reacting with formate to generate CO_2 and H_2O, and so on.[28−31] Accordingly, considering the unique properties of TiO_2(B), it is urgent and meaningful to conduct related research on the TiO_2(B)-supported catalyst for HCHO oxidation.

In the present work, mesoporous TiO_2(B) was used as the support to load Pt nanoparticles (NPs) for synthesizing the HCHO oxidation catalyst (denoted as Pt/TiO_2(B)). As expected, the Pt/TiO_2(B) catalyst exhibited better HCHO oxidation performance than Pt NPs supported on anatase, rutile TiO_2, and P25. The structural properties of various catalysts were systematically studied by Raman spectroscopy, X-ray photoelectron spectroscopy (XPS), Brunauer−Emmett−Teller (BET) analysis, scanning electron microscopy (SEM), transmission electron microscopy (TEM), CO-diffuse reflectance infrared Fourier transformed spectroscopy (DRIFTS), and so on. Simultaneously, the structure−performance relationship discussion was supported by HCHO-DRIFTS analyses.

2. RESULTS AND DISCUSSION

2.1. Overall Structural Properties of Catalysts. The XRD pattern and Raman spectrum of the Pt/TiO_2(B) catalyst are displayed in Figure 1. There are six obvious peaks at 2θ = 25.0°, 28.7°, 29.9°, 33.3°, 37.8°, 43.6°, and 48.5°, as shown from the XRD pattern in Figure 1a. These peaks are ascribed to the (110), (002), (−401), (310), (003), and (020) reflections of the TiO_2(B) phase, respectively (PDF#35-0088). The characteristic peak of Pt species is not observed in the XRD pattern, suggesting the good dispersion of Pt NPs in the Pt/TiO_2(B) catalyst.[32] It is acknowledged that the Raman technique is more sensitive than XRD in detecting the crystal information of TiO_2(B).[33] In the Raman spectrum of Pt/TiO_2(B) presented in Figure 1b, the main modes at 122, 197, 241, 248, 364, 407, 431, 468, 636, and 654 cm^{-1} are the direct expression of the corresponding characteristic Raman vibrations of the TiO_2(B) phase.[26,33] The signal related to the anatase phase could not be observed in the Raman spectrum, which indicates that the support of Pt/TiO_2(B) consists of pure TiO_2(B) only.

Figure 2 displays nitrogen adsorption−desorption isotherms and pore size distributions of Pt/TiO_2(B). The catalyst Pt/

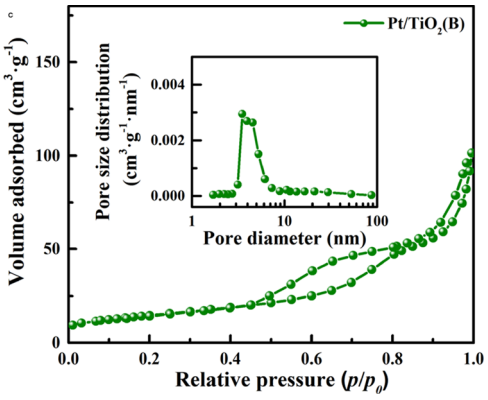

Figure 2. Nitrogen adsorption−desorption isotherms and pore size distributions (inserted diagram) of the Pt/TiO_2(B) catalyst.

TiO_2(B) has a type IV isotherm with a H3 hysteresis loop in a relative pressure p/p_0 range of 0.4−0.6, suggesting the mesoporous structure of the Pt/TiO_2(B) catalyst. As shown in Figure S1, all control catalysts exhibited type IV isotherms and possessed mesoporous structures.[34] The inset in Figure 2 displays that the most probable pore size of the Pt/TiO_2(B) catalyst is about 3.9 nm and its pore size distribution is relatively uniform. Furthermore, the detailed pore structural data of catalysts are shown in Table 1. The specific surface area of Pt/TiO_2(B) is 53.0 $m^2\ g^{-1}$, slightly higher than that of the control catalysts (40.1 $m^2\ g^{-1}$ for Pt/anatase, 30.6 $m^2\ g^{-1}$ for Pt/rutile, and 41.0 $m^2\ g^{-1}$ for Pt/P25). In addition, the pore volume of the Pt/TiO_2(B) catalyst is 0.16 $cm^3\ g^{-1}$, comparable to those of the control catalysts (0.14−0.40 $cm^3\ g^{-1}$).

https://doi.org/10.1021/acsomega.2c02490
ACS Omega 2022, 7, 25491−25501

Table 1. Comparison in Porous Structural Data and Reaction Rate of Pt/TiO_2(B) with Control Samples

catalyst	S_{BET} ($m^2\ g^{-1}$)	V_P ($cm^3\ g^{-1}$)	D_P (nm)	crystal phase	metal type and amount	T (°C)	C_0 (ppm)/GHSV (h^{-1})	reaction rate ($\mu mol_{HCHO}\ g^{-1}_{cat}\ s^{-1}$)	reference
Pt/TiO_2(B)	53.0	0.16	8.5	TiO_2(B)	0.5% Pt	30	180/54,000	15.8	present work
Pt/anatase	40.1	0.40	19.5	anatase	0.5% Pt	30	180/54,000	1.89	present work
Pt/rutile	30.6	0.14	7.6	rutile	0.5% Pt	30	180/54,000	3.53	present work
Pt/P25	41.0	0.28	22.8	anatase/rutile	0.5% Pt	30	180/54,000	2.84	present work
Pt/TiNT	31.6			anatase	0.4% Pt	30	50/30,000	4.42	35
Pt/P25	51.1			anatase/rutile	0.4% Pt	30	50/30,000	0.84	36
Pt/TiO_2	47.4			anatase	0.5% Pt	20	100/50,000	3.10	37
Pt/TiO_2				rutile	1.0% Pt	40	375/60,000	1.40	38
Ag/TiO_2	35.3	0.30	27.4	anatase	8.0% Ag	35	130/10,0000	0.11	39
Pt/ZSM-5	326.1			ZSM-5	0.4% Pt	30	50/30,000	1.36	40
Pd/TiO_2	57.2			anatase/rutile	1.0% Pd	25	140/95,000	1.65	16
Pt/Fe_2O_3				α-Fe_2O_3	2.4% Pt	30	400/60,000	10.61	41
Ag/SBA-15	520.6	0.81	6.2	amorphous	7.0% Ag	30	1000/15,000	0.29	42
Au/Al_2O_3				γ-Al_2O_3	3.5% Au	30	500/35,400	2.51	43
Au/CeO_2	130.0	0.21	3.4	fluorite	1.0% Au	25	200/55,000	4.09	44

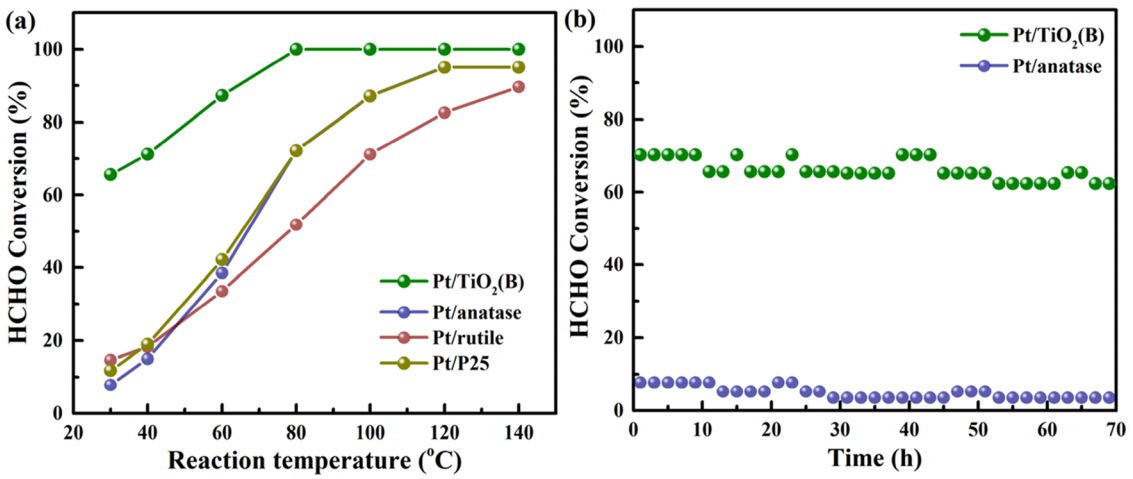

Figure 3. HCHO conversion as a function of reaction temperature (a) and long-term reaction results (b) of Pt/TiO_2(B) and various control samples.

2.2. Formaldehyde Decomposition Performance. Figure 3a shows the HCHO conversion of various catalysts as a function of reaction temperature. From 30 to 140 °C, the HCHO conversion of Pt/TiO_2(B) is invariably higher than those of anatase, rutile, and P25 TiO_2-supported Pt catalysts. Note that the HCHO conversion of Pt/TiO_2(B) can reach 65% at 30 °C (i.e., room temperature), while those of the three control samples are only between 5 and 15%, indicating the excellent room-temperature HCHO oxidation performance of Pt/TiO_2(B). As listed in Table 1, the corresponding HCHO oxidation rate of Pt/TiO_2(B) is 4.5−8.4 times as high as that of Pt/anatase, Pt/rutile, and Pt/P25. Pt/TiO_2(B) can achieve complete conversion of HCHO at 80 °C under the present experimental conditions. By comparison, the reaction temperatures of HCHO complete conversion on all control catalysts are above 140 °C. The HCHO conversion of Pt/anatase is slightly higher than that of Pt/rutile, but both of which are obviously lower than that of Pt/TiO_2(B). Apparently, mesoporous TiO_2(B) as the support has a significant advantage in catalytically oxidizing HCHO at room temperature, as confirmed by the superior reaction rate of Pt/TiO_2(B) to those in the reported literature (as seen in Table 1).

In general, the pore structure of catalysts directly influences the transport of reactants/resultants and the dispersion state of active species during catalyst preparation.[21,45,46] Accordingly, the catalytic performance of Pt/TiO_2(B) was preliminarily analyzed with the pore structure data of catalysts. The porous structural data in Table 1 show that the specific surface area of Pt/TiO_2(B) is somewhat larger than those of Pt/anatase, Pt/rutile, and Pt/P25, while the pore volume value of Pt/TiO_2(B) is between them. According to the similar porous properties of Pt/TiO_2(B) and control samples, it could be determined that the geometrical factor of Pt/TiO_2(B) is not the main factor for its excellent room-temperature HCHO oxidation performance.

Moreover, it can also be concluded from the above data that the structural properties and catalytic performance between the anatase TiO_2-supported Pt catalyst and rutile TiO_2-supported one are different but not significant. The catalytic differences between them have been discussed previously.[20,47] Thus, in the following content, Pt/anatase is selected as the primary control sample for comparatively studying the unique structural and

https://doi.org/10.1021/acsomega.2c02490
ACS Omega 2022, 7, 25491−25501

catalytic characteristics of Pt/TiO_2(B). Figure 3b displays the results of the long-term reaction of HCHO oxidation of Pt/TiO_2(B) and Pt/anatase. Generally, there is only slight fluctuation in HCHO conversion of Pt/TiO_2(B) and no significant deactivation during the process of stability evaluation, which is consistent with the results of Pt/anatase. This manifests the excellent long-term HCHO oxidation performance of Pt/TiO_2(B) at room temperature.

2.3. Dispersion State of Pt Species. Field-emission scanning electron microscopy (FESEM) and TEM images of Pt/TiO_2(B) are shown in Figure 4. Varied from spheroidal

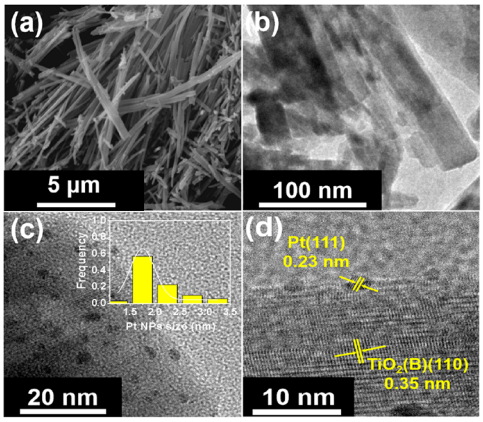

Figure 4. FESEM image (a) and TEM images (b–d) of Pt/TiO_2(B). The inset is the size distribution of Pt NPs of Pt/TiO_2(B).

particles of Pt/anatase (Figure S2), Pt/TiO_2(B) (Figure 4a) exhibits a whisker structure with several micrometers in length and a few dozen to 200 nm in diameter. As displayed from the TEM image in Figure 4b, Pt/TiO_2(B) has an identical morphology to that in the FESEM image. The high-resolution TEM image in Figure 4c clearly shows that numerous dark spots are evenly dispersed in the Pt/TiO_2(B) catalyst. One of the spots is randomly chosen to analyze its fringe patterns (Figure 4d). The lattice fringe spacing is 0.23 nm, which matches with the (111) plane of metallic Pt. Hence, all the dark spots can be identified as the Pt NPs. The element mapping shown in Figure S3 also confirms the good dispersion of Pt NPs on the catalyst surface. Moreover, the lattice fringe spacing of the support nearby Pt NP is 0.35 nm, which is assigned to the (110) plane of TiO_2(B),[22,26] further confirming the Raman and XRD analyses.

The statistical result of the Pt NP size of Pt/TiO_2(B) inserted in Figure 4c shows that the most probable particle size of Pt NPs of Pt/TiO_2(B) is ca. 1.8 nm, slightly smaller than that of Pt/anatase (2.2 nm, as seen in Figure S2). This indicates that Pt NPs can be well dispersed on both TiO_2(B) and anatase, which is consistent with the above XRD analyses. The detailed structural properties of Pt NPs are further analyzed by CO-DRIFTS. Figure 5 displays that both Pt/TiO_2(B) and Pt/anatase have two distinct bands at 2056 and 2078 cm^{-1}, which are assigned to the linear adsorption of CO on step and terrace sites of Pt NPs, respectively.[48−50] The similar shape in CO-DRIFT spectra between Pt/TiO_2(B) and Pt/anatase indicates their analogous morphology of Pt NPs,[51] which is consistent with the observation by HRTEM analyses. Furthermore, the degree of Pt dispersion could be calculated according to the sphere model,[52] and the detailed process is described in the Supporting Information. Based on this, the

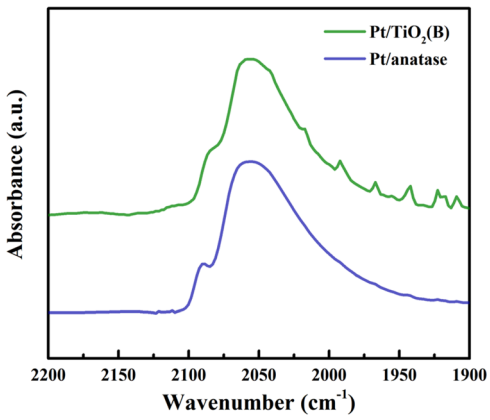

Figure 5. CO-DRIFT spectra of Pt/TiO_2(B) and Pt/anatase.

TOF values of catalysts can be obtained and those of Pt/TiO_2(B) and Pt/anatase are 4.4×10^{-3} and 0.65×10^{-3} s^{-1}, respectively.[53] The dramatically higher TOF value indicates that Pt/TiO_2(B) possesses higher intrinsic activity in room-temperature HCHO oxidation than Pt/anatase, which suggests the presence of different active sites for HCHO oxidation between Pt/TiO_2(B) and Pt/anatase.

The analyses in chemical valence of Pt NPs of Pt/TiO_2(B) and Pt/anatase are presented in Figure 6a. All the XPS Pt 4f spectra could be divided into three 4f7/2-4f5/2 doublets at binding energies of 71.1−74.4, 72.3−75.6, and 73.8−77.1 eV assigned to Pt^0, Pt^{2+}, and Pt^{4+} species, respectively.[54,55] The content of corresponding species can be estimated by the area of the resolved peak, which is used to identify the chemical valent state of Pt NPs of the two catalysts. The percentage contents of Pt^0, Pt^{2+}, and Pt^{4+} species of Pt/TiO_2(B) are 10.3, 64.0, and 25.6%, respectively, while those of Pt/anatase are 37.7, 41.7, and 20.6%, respectively. Pt/TiO_2(B) contains a higher content of oxidized $Pt^{\delta+}$ species than Pt/anatase does, especially for Pt^{2+}.

As seen in Figure 7, temperature-programmed reduction (TPR) patterns of both Pt/TiO_2(B) and Pt/anatase display two reduction stages from room temperature to 150 °C and from 200 to 300 °C, which are ascribed to the reduction of oxidized Pt species and Pt-support boundary species, respectively.[19,56] According to the reduction temperature of various species provided by TPR patterns, it is confirmed that all oxidized Pt species of two catalysts can be completely reduced to metallic Pt species under the preparation conditions. Moreover, the reduction temperature of Pt/TiO_2(B) is not dramatically different from those of Pt/anatase, which demonstrates that the interaction of Pt species with TiO_2(B) is the same as that with anatase. Additionally, the XPS spectra of Ti 2p of the catalysts in Figure 6c show that the binding energies of Ti ions in both Pt/TiO_2(B) and Pt/anatase are the same; that is, a similar state of oxygen vacancies around Pt species to the Pt/anatase should exist in the Pt/TiO_2(B).[32] Thus, it is inferred that the presence of adsorbed species on Pt species may be the main reason for the different chemical valent states of Pt NPs between Pt/TiO_2(B) and Pt/anatase, because the reduced catalysts inevitably come into contact with air and moisture during the transfer and preservation. It is required to comparatively analyze the state of adsorbed species on the surface of Pt/TiO_2(B) and Pt/anatase.

Figure 6b shows the XPS O 1s spectra of Pt/TiO_2(B) and Pt/anatase. Both of them have three deconvoluted peaks at

https://doi.org/10.1021/acsomega.2c02490
ACS Omega 2022, 7, 25491−25501

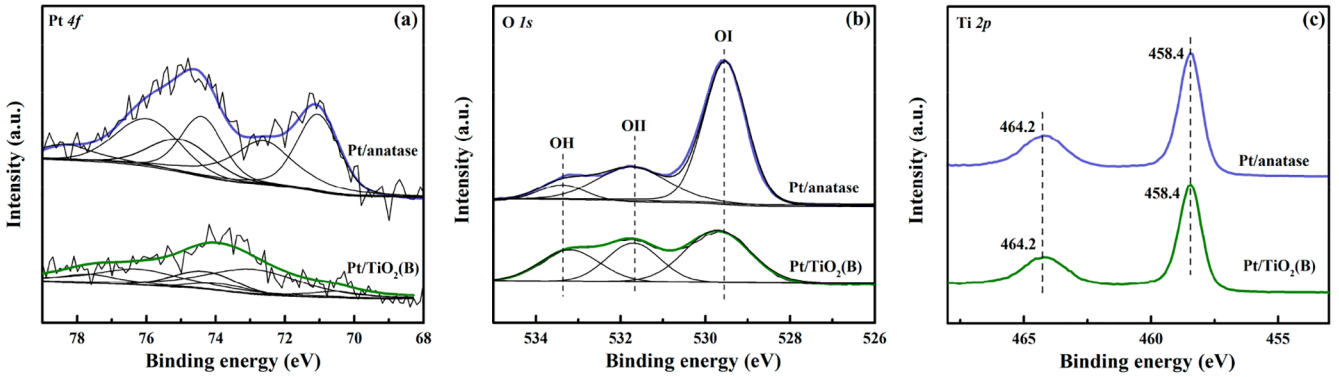

Figure 6. XPS spectra for Pt 4f (a), O 1s (b), and Ti 2p (c) of $Pt/TiO_2(B)$ and Pt/anatase.

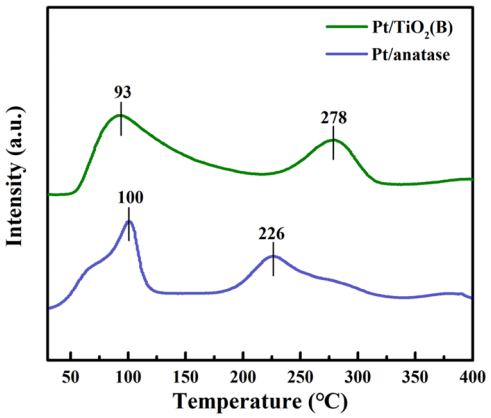

Figure 7. H_2 temperature-programmed reduction (H_2-TPR) patterns of $Pt/TiO_2(B)$ and Pt/anatase.

binding energies of 529.7, 532.0, and 533.5 eV, which are attributed to the bulk lattice oxygen (O_I), surface oxygen species (O_{II}), and surface hydroxyl oxygen (OH), respectively.[48,57,58] The ratios of O_{II}/O_I to OH/O_I are calculated by the peak areas of O_I, O_{II}, and OH, which are useful when analyzing the amount of hydroxyls and oxygen species on the two catalysts. The OH/O_I ratios of $Pt/TiO_2(B)$ and Pt/anatase are 0.615 and 0.126, respectively. Moreover, the O_{II}/O_I ratio of $Pt/TiO_2(B)$ is 0.609, higher than that of Pt/anatase (0.424). Unsurprisingly, the amounts of hydroxyls and oxygen species on $Pt/TiO_2(B)$ and Pt/anatase are different. Because there are more hydroxyls and oxygen species on $Pt/TiO_2(B)$, the different chemical valent Pt species between $Pt/TiO_2(B)$ and Pt/anatase as mentioned above can be explained.

The amount of oxygen species is generally considered to be one of the key factors directly influencing the HCHO oxidation performance of catalysts.[20,50,59] The large amount of oxygen species must be one of the pieces of evidence of highly efficient HCHO oxidation on $Pt/TiO_2(B)$. As for the increment in the amount of oxygen species of $Pt/TiO_2(B)$ relative to Pt/anatase, it is unlikely to be related to their dispersion states of Pt NPs as they have the same

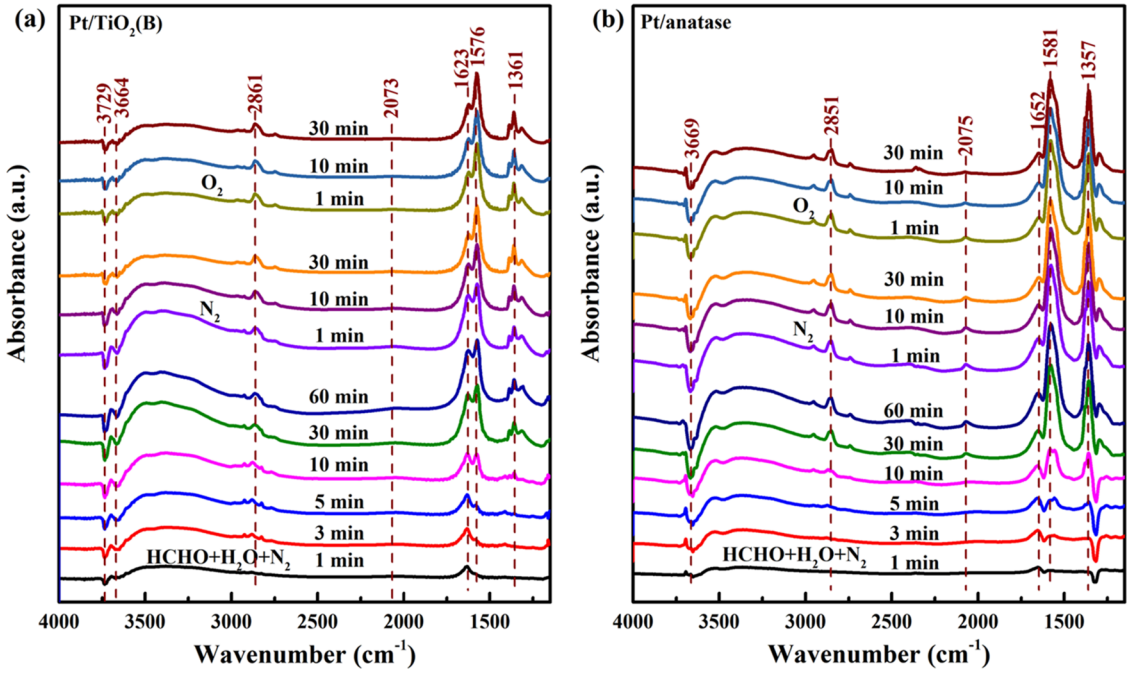

Figure 8. Dynamic changes of in situ HCHO-DRIFT profiles of $Pt/TiO_2(B)$ (a) and Pt/anatase (b) at the atmospheres of HCHO + N_2 + H_2O, N_2, and O_2.

https://doi.org/10.1021/acsomega.2c02490
ACS Omega 2022, 7, 25491−25501

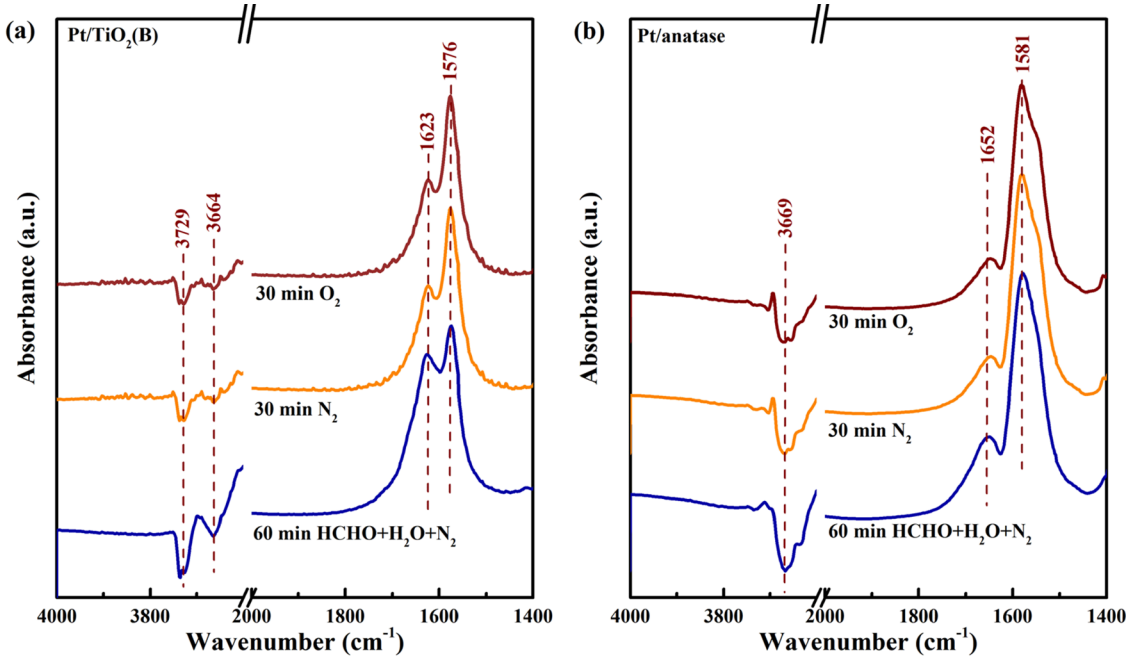

Figure 9. Partial enlarged image of the DRIFT spectra of $Pt/TiO_2(B)$ (a) and Pt/anatase (b).

morphological structure of Pt NPs according to the HRTEM and CO-DRIFTS analyses. Alternatively, the increasing content of oxygen species on $Pt/TiO_2(B)$ could be attributed to the possession of a large number of hydroxyls. With the hydroxyl-rich supports or in a high-humidity environment, the corresponding catalysts could achieve the markedly increased content of oxygen species.[28,31,60] It is well accepted that hydroxyls can facilitate the adsorption and diffusion of O_2 to active sites and consequently improve the oxygen activation.[30,61]

In addition to assisting oxygen activation, the hydroxyls can enhance the adsorption ability of HCHO on the catalyst due to their good affinity to HCHO molecules by the formation of hydrogen bonds.[62,63] In addition, the hydroxyls themselves can participate in the HCHO oxidation process. Hong et al. found that under anaerobic conditions (where oxygen was absent), the reaction of HCHO oxidation can still be performed in the presence of moisture.[31] Additionally, He et al. discovered that hydroxyls could react with formate (an intermediate of HCHO oxidation) to generate the carbonate/bicarbonate, which significantly improved the HCHO oxidation efficiency of the catalyst.[6] Hence, there is no doubt that $Pt/TiO_2(B)$ with abundant hydroxyls possesses such excellent HCHO oxidation performance.

2.4. Mechanism Discussion. The oxidation of HCHO is successively experienced through the intermediate species of dioxymethylene (DOM), formate ($HCOO^-$), and CO, and finally being oxidized into CO_2.[37,64] According to data analyzed above, although a high overall reaction rate of HCHO oxidation can be obtained on $Pt/TiO_2(B)$, it is still unclear which step of HCHO oxidation is improved. The understanding of this question is crucial for exploring the structure−activity relationship of catalysts and their further development. Herein, in situ HCHO-DRIFTS was used to detect the intermediate species of HCHO oxidation on the surface of various catalysts to study the differences in the reaction mechanisms between $Pt/TiO_2(B)$ and Pt/anatase.

In the initial stage, a mixed gas flow of HCHO, H_2O, and N_2 is injected into the in situ chamber. As shown in Figure 8a, the bands at around 1361 and 1576 cm^{-1} are assigned to the symmetric stretching vibration and the asymmetric stretching vibration of formate.[37,65] Moreover, the symmetric vibration of the $-CH_2-$ group at around 2861 cm^{-1} corresponding to DOM can also be observed,[66] demonstrating that the HCHO decomposition process from HCHO to formate via DOM also occurs on $Pt/TiO_2(B)$, which accords with that on Pt/anatase (as seen in Figure 8b). It is noteworthy that the signal intensity of the CO band at 2073 cm^{-1} is very weak in various DRIFT spectra of $Pt/TiO_2(B)$, while the intensity of the CO signal on Pt/anatase is obviously strong. After N_2 purging in the second stage and O_2 purging in the third stage, no signal about other new species arises in the DRIFT spectra of $Pt/TiO_2(B)$ and Pt/anatase. Apparently, the appearance of the signal of all intermediate species in DRIFT spectra demonstrates that the oxidation of HCHO on $Pt/TiO_2(B)$ follows the reaction pathway of HCHO → DOM → $HCOO^-$ → CO → CO_2, which is consistent with that of Pt/anatase.

Subsequently, the state of hydroxyls of two catalysts is further analyzed by comparing the hydroxyl-related signals in HCHO-DRIFT spectra. The magnified DRIFT spectra in Figure 9 display that the bending vibrations of adsorbed water molecules ($\delta(H_2O)$) on $Pt/TiO_2(B)$ appear at a wavenumber of 1623 cm^{-1}, while the corresponding wavenumber of Pt/anatase is 1652 cm^{-1}. The red shift in the wavenumber of $\delta(H_2O)$ is attributed to the increased interaction of H_2O molecules with the substrate.[25,68] This suggests that $Pt/TiO_2(B)$ could have better affinity to water molecules than Pt/anatase, which is beneficial to increasing the adsorption of water on $Pt/TiO_2(B)$, as also demonstrated by its obviously higher signal intensity of bending vibrations of $\delta(H_2O)$. As mentioned above, H_2O is liable to dissociate into hydroxyl on $TiO_2(B)$.[25] Hence, the characteristics of enhanced H_2O adsorption and dissociation can endow $Pt/TiO_2(B)$ with a large number of hydroxyls, echoing with the above XPS analyses.

https://doi.org/10.1021/acsomega.2c02490
ACS Omega 2022, 7, 25491−25501

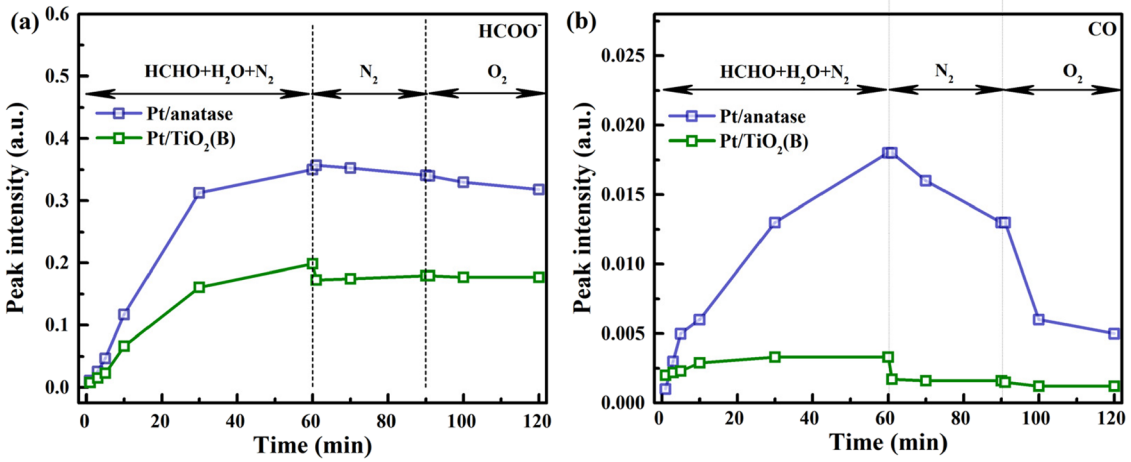

Figure 10. DRIFTS signal intensities of formate (a) and CO (b) as a function of time on $Pt/TiO_2(B)$ and Pt/anatase.

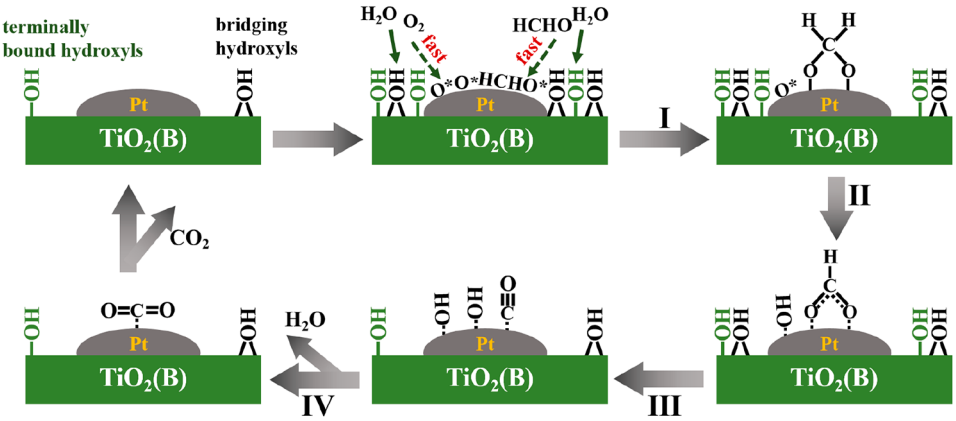

Figure 11. Scheme for HCHO oxidation on $Pt/TiO_2(B)$.

Moreover, Figure 8 shows that the DRIFT spectra of both $Pt/TiO_2(B)$ and Pt/anatase have the negative peaks in the range of 3600−3800 cm^{-1}, which are assigned to the stretching vibration of hydroxyls. These negative peaks have been regarded as evidence of hydroxyl involvement in HCHO oxidation.[6,31,69] As clearly displayed in Figure 9b, there is one negative peak at 3669 cm^{-1} in this region of DRIFT spectra of Pt/anatase, corresponding to bridging hydroxyls.[68,70] This indicates that the bridging hydroxyl-involved HCHO oxidation mechanism is followed on Pt/anatase, in accordance with many previous reports.[6,13,15] Dissimilarly, the DRIFT spectra of $Pt/TiO_2(B)$ (as seen in Figure 9a) show two negative peaks at 3729 and 3664 cm^{-1}, ascribed to terminally bound hydroxyls and bridging hydroxyls, respectively.[68,70] It is confirmed that two types of hydroxyls participate in the HCHO oxidation on $Pt/TiO_2(B)$. Moreover, the intensity of terminally bound hydroxyls is obviously stronger than that of bridging hydroxyls, suggesting the dominant role played by the terminally bound hydroxyls in the HCHO oxidation of $Pt/TiO_2(B)$.

To the best of our knowledge (see the survey results in Table S1), the reports about the bridging hydroxyl involvement in the HCHO oxidation account for the majority, while very rare reports record the terminally bound hydroxyls or both. The type of hydroxyl as a factor influencing the HCHO oxidation performance receives little attention. Several studies have shown that the bridging hydroxyls interacted with HCHO to form DOM, and subsequently the terminally bound hydroxyls promoted the formation of formate from DOM through the Cannizzaro mechanism, and the latter reaction was considered to be thermodynamically and kinetically favorable.[66,67] This indicates that the synergetic involvement of bridging hydroxyls and terminally bound hydroxyls in HCHO oxidation is essential for elevating the reaction rates of HCHO → DOM → $HCOO^-$. That is to say, the first two steps of HCHO oxidation can be accelerated over $Pt/TiO_2(B)$.

Further comparative analysis is conducted on the signal intensity of the other two key intermediate species (about 1580 cm^{-1} for formate and 2075 cm^{-1} for CO) as a function of experimental time, as plotted in Figure 10. During the initial stage of HCHO + H_2O + N_2 injection, the signal ascribed to formate is gradually enhanced, indicating that the formate increasingly accumulates on the surface of the two catalysts. As reported previously, the formate decomposition was the slowest step in formaldehyde oxidation, so the signal of formate was the most obvious in HCHO-DRIFT spectra compared with other intermediate species, and its rate was considered to be the rate-limiting step of HCHO oxidation.[6,37] In the second and third stages, the signal intensity of formate of both catalysts decreases slightly, indicating difficulty in decomposing the formate under the condition of only oxygen but no hydroxyl.[31] Thus, hydroxyls are essential for the fast formate decomposition. By comparison, the signal intensity of formate of $Pt/TiO_2(B)$ is always weaker than that of Pt/anatase during the whole experimental process, suggesting that

https://doi.org/10.1021/acsomega.2c02490
ACS Omega 2022, 7, 25491−25501

the formate is not easy to accumulate on Pt/TiO_2(B). As mentioned above, the coparticipation of two hydroxyl groups in HCHO oxidation can accelerate the formation of formate. Therefore, the weak signal intensity of formate in DRIFT spectra of Pt/TiO_2(B) could be caused by the rapid decomposition of formate rather than the slow generation.

Moreover, as seen in Figure 10b, the CO signal intensity of Pt/anatase increases slowly with the emergence of formate and then decreases after O_2 is introduced. The slow increase in CO signal intensity demonstrates the difficult decomposition of formate into CO. Additionally, the CO signal intensity begins to decrease with N_2 purge, corresponding to the oxidation of CO by oxygen species on Pt/anatase. This indicates that the further reaction of CO has actually proceeded from the first stage. After pure O_2 injection, the CO signal intensity decreases to a low value. Different from Pt/anatase, the CO signal of Pt/TiO_2(B) has insignificant intensity at the first stage and instantly disappears upon stopping the HCHO injection. Obviously, the consumption rate of CO on Pt/TiO_2(B) significantly exceeds the generation rate of CO from formate. This could be attributed to the existence of more oxygen species on Pt/TiO_2(B) as analyzed by the above XPS measurement. Moreover, the hydroxyls on Pt/TiO_2(B) can also contribute to the transport of CO species due to the weakened interaction between CO and the hydroxylated surface.[71,72]

Based on the above analyses and discussion, the role of hydroxyls in HCHO oxidation of Pt/TiO_2(B) is clarified. As shown in Figure 11, the presence of abundant hydroxyls is beneficial to oxygen activation for formation of more active species on Pt/TiO_2(B). Moreover, two types of hydroxyls (bridging hydroxyl and terminally bound hydroxyl) are synergistically involved in the HCHO oxidation, which effectively improves the reactions of formaldehyde to DOM and DOM to formate with Pt as the active site. Additionally, hydroxyls also contribute to the fast decomposition of formate and consequently avoid the accumulation of excessive formate on Pt/TiO_2(B). Finally, the formed CO is liable to be transported to active sites on the hydroxylated surface and rapidly oxidized by a large number of reactive oxygen species on the Pt. It is noteworthy that all the steps of HCHO oxidation are connected in series, and consequently the delay in any step will result in a decrease in the overall reaction rate of HCHO oxidation. By consecutively analyzing each HCHO oxidation step, it can be determined that the reaction rate of all steps of HCHO oxidation on Pt/TiO_2(B) is accelerated, which explains the excellent catalytic performance of Pt/TiO_2(B).

3. CONCLUSIONS

In the present work, a mesoporous TiO_2(B)-supported Pt catalyst was prepared to first apply in the HCHO oxidation. The as-synthesized Pt/TiO_2(B) catalyst not only exhibited superior HCHO oxidation performance to other crystalline TiO_2-supported Pt catalysts, but also demonstrated excellent catalytic stability. The roles of hydroxyls in different steps of HCHO oxidation were analyzed successively, and it was found that all steps could be accelerated. The hydroxyls on Pt/TiO_2(B) significantly contributed to improving the HCHO oxidation performance.

4. EXPERIMENTAL SECTION

4.1. Chemicals and Catalyst Preparation. Anhydrous potassium carbonate (K_2CO_3), anhydrous calcium chloride ($CaCl_2$), and chloroplatinic acid ($H_2PtCl_6{\cdot}6H_2O$) were purchased from Sinopharm Chemical Reagent Co., Ltd. Nitric acid (HNO_3) was purchased from Chemical Reagent Co., Ltd. Anatase TiO_2 was purchased from Jingrui New Material Co., Ltd. Rutile TiO_2 was purchased from Nano New Material Technology Co., Ltd. P25 was purchased from Evonik Degussa (China) Co., Ltd. $TiO_2{\cdot}nH_2O$ was provided by Jiangsu Taibai Group Co., Ltd. All the chemicals were used as received.

Mesoporous TiO_2(B) was synthesized according to the procedures as described in our previous work.[26,73] Briefly, potassium titanate ($K_2Ti_2O_5$) was preliminarily prepared by calcination from a mixture of K_2CO_3 and $TiO_2{\cdot}nH_2O$ in a Ti/K molar ratio of 0.95 at 860 °C for 4 h. Then, the $K_2Ti_2O_5$ powders were separately placed in an autoclave filled with $CaCl_2$ saturated solution for being treated at 180 °C. After 24 h, the powders were ion-exchanged to remove potassium ions by HNO_3 aqueous solution (pH = 2). The collected powders were calcined at 500 °C for 2 h to achieve the mesoporous TiO_2(B). The content of potassium residual was below 0.2 wt % according to previous work,[22] most of which were distributed in the subsurface of mesoporous TiO_2(B) due to no detection on potassium by XPS analyses.

Loading of Pt NPs (0.5 wt %) on mesoporous TiO_2(B) was carried out by wet impregnation using H_2PtCl_6 as the precursor. The impregnated powders were calcined in air at 500 °C for 2 h and subsequently reduced in H_2 at 300 °C for 2 h to obtain the Pt/TiO_2(B) catalyst. For comparison, anatase TiO_2, rutile TiO_2, and P25 were used as control samples and their corresponding catalysts were denoted as Pt/anatase, Pt/rutile, and Pt/P25, respectively.

4.2. Characterization. The Raman spectrum of TiO_2(B) was provided by a Horiba HR 800 spectrometer equipped with a CCD camera detector with the wavelength of excitation light of λ = 514 nm. The signal was sampled in the range from 100 to 800 cm^{-1}. Nitrogen adsorption−desorption isotherms at −196 °C of various catalysts were measured on an ASAP2020 physisorption analyzer (Micromeritics, USA). The surface area (S_{BET}) of catalysts was calculated using the BET model, and the pore volume (V_P) was obtained by nitrogen adsorption with a relative pressure of 0.99. Pore size distribution was determined by the Barrett−Joyner−Halenda model. Nanoscale morphology of catalysts was provided by field-emission scanning electron microscopy (FESEM, JEM-7600 F) and high-resolution transmission electron microscopy (HRTEM, JEM-2010). X-ray photoelectron spectroscopy (XPS, ESCALAB 250) equipped with a monochromatic Al Kα X-ray beam was utilized to study the chemical state of various elements on the surface of the catalyst. The binding energies of elements were referenced to the C 1s peak (284.6 eV) of adventitious hydrocarbons. H_2-TPR experiments were carried out in a TP-5000 micro fixed-bed flow system. Before the test, the catalyst powders (0.1 g) were pretreated in a flow of air (30 mL·min^{-1}) at 500 °C for 0.5 h followed by cooling to room temperature. The atmosphere of the system was switched to a mixed gas of 10% H_2/N_2. After stable flow for 0.5 h, the system started to be heated to 500 °C at a heating rate of 10 °C·min^{-1}. The H_2 consumption during the test was monitored by the TCD detector.

https://doi.org/10.1021/acsomega.2c02490
ACS Omega 2022, 7, 25491−25501

In situ diffuse reflectance infrared Fourier transformed spectroscopy (in situ DRIFTS) was performed on a Nicolet-6700 spectroscope apparatus (Thermo Electron) equipped with a diffuse reflectance accessory and an MCT detector. Herein, the DRIFTS test contained HCHO-DRIFTS and CO-DRIFTS depending on different adsorbents. The operational processes of HCHO-DRIFTS were taken to investigate the reaction path of HCHO oxidation over various catalysts. The as-prepared catalyst powders were placed in the in situ chamber and pretreated at 300 °C for 0.5 h in the atmosphere of nitrogen with a flowing rate of 30 mL·min^{-1}. After being cooled down to 30 °C, the chamber was introduced with a mixed gas stream of HCHO + H_2O + N_2, which was produced by bubbling. After 1 h, pure N_2 and pure O_2 passed through the chamber sequentially to study the consumption and oxidation of different intermediates. The spectra under reaction conditions were recorded after 32 scans with a resolution of 4 cm^{-1}. Moreover, CO-DRIFTS was used to analyze the dispersion state of Pt NPs. The catalyst was in situ reduced in 10% H_2/N_2 at 300 °C for 0.5 h and cooled down to 30 °C in an N_2 gas flow. Then, CO was introduced into the chamber. After 0.5 h, the excessive and weakly adsorbed CO was removed by being purged with a flowing pure N_2 stream. The spectra from 1900 to 2200 cm^{-1} were recorded after 32 scans with a resolution of 4 cm^{-1}.

4.3. Catalytic Evaluation. The HCHO oxidation reaction was carried out in a fixed-bed flow reactor. Catalyst powders were added in a quartz tube with an inner diameter of 6 mm. The feed gas consisted of 180 ppm HCHO, H_2O vapor (relative humidity of 35%), 20 vol % O_2, and balance N_2, produced by passing air stream through a bubbler containing a 37% HCHO aqueous solution in bath at 4 °C. The gas hourly space velocity for each experiment was 54,000 h^{-1}. During the reaction, the reaction temperature of HCHO oxidation was controlled between 30 and 140 °C by a temperature-programmed furnace. The HCHO concentrations of feed gas and exhaust gas were analyzed online by a gas chromatograph, which were synchronously checked by the CO_2 detector. No CO was detected in exhaust gas by the CO detector. The sample was analyzed after at least 30 min of stable reaction. HCHO conversion of various catalysts was calculated according to the change of HCHO concentration in the feed gas and exhaust gas.

■ ASSOCIATED CONTENT

Supporting Information

The Supporting Information is available free of charge at https://pubs.acs.org/doi/10.1021/acsomega.2c02490.

Nitrogen adsorption−desorption isotherms and pore size distributions of control samples, TEM images and size distribution of Pt nanoparticles of Pt/anatase, scanning electron microscopy−energy-dispersive X-ray spectroscopy elemental mapping of Pt/TiO_2(B), calculation of the degree of Pt dispersion and TOF value, and investigation of bridging hydroxyls and terminally bound hydroxyls in DRIFTS of catalysts in other literature studies (PDF)

■ AUTHOR INFORMATION

Corresponding Author

Licheng Li − *Jiangsu Co-Innovation Center of Efficient Processing and Utilization of Forest Resources, College of Chemical Engineering, Nanjing Forestry University, Nanjing 210037, P. R. China;* orcid.org/0000-0001-8501-6981; Email: llc0024@yahoo.com, lilc@njfu.edu.cn

Authors

Tongtong Wei − *Jiangsu Co-Innovation Center of Efficient Processing and Utilization of Forest Resources, College of Chemical Engineering, Nanjing Forestry University, Nanjing 210037, P. R. China*

Xuejuan Zhao − *School of Materials Science and Engineering, Nanjing Institute of Technology, Nanjing 211167, P. R. China*

Long Li − *Jiangsu Co-Innovation Center of Efficient Processing and Utilization of Forest Resources, College of Chemical Engineering, Nanjing Forestry University, Nanjing 210037, P. R. China*

Lei Wang − *Jiangsu Co-Innovation Center of Efficient Processing and Utilization of Forest Resources, College of Chemical Engineering, Nanjing Forestry University, Nanjing 210037, P. R. China*

Shenjie Lv − *Jiangsu Co-Innovation Center of Efficient Processing and Utilization of Forest Resources, College of Chemical Engineering, Nanjing Forestry University, Nanjing 210037, P. R. China*

Lei Gao − *Jiangsu Architectural Decoration Integrated Installation Engineering Technology Research Center, Nanjing Guohao Decoration & Installation Engineering Co., Ltd., Nanjing 210012, P. R. China*

Gaosong Yuan − *Jiangsu Architectural Decoration Integrated Installation Engineering Technology Research Center, Nanjing Guohao Decoration & Installation Engineering Co., Ltd., Nanjing 210012, P. R. China*

Complete contact information is available at: https://pubs.acs.org/10.1021/acsomega.2c02490

Notes

The authors declare no competing financial interest.

■ ACKNOWLEDGMENTS

This work was financially supported by the General Program of National Natural Science Foundation of China (21978134), the Natural Science Foundation of Jiangsu Province (BK20191392), and the Project of Jiangsu Provincial Building Decoration Integrated Installation Engineering Technology Research Center (BM2019210).

■ REFERENCES

(1) Zhu, L.; Jacob, D. J.; Keutsch, F. N.; Mickley, L. J.; Scheffe, R.; Strum, M.; González Abad, G.; Chance, K.; Yang, K.; Rappenglück, B. Formaldehyde (HCHO) as a hazardous air pollutant: Mapping surface air concentrations from satellite and inferring cancer risks in the United States. *Environ. Sci. Technol.* **2017**, *51*, 5650−5657.

(2) Salthammer, T.; Mentese, S.; Marutzky, R. Formaldehyde in the Indoor Environment. *Chem. Rev.* **2010**, *110*, 2536−2572.

(3) Guo, J.; Lin, C.; Jiang, C.; Zhang, P. Review on noble metal-based catalysts for formaldehyde oxidation at room temperature. *Appl. Surf. Sci.* **2019**, *475*, 237−255.

(4) Zhang, Z.; Jiang, Z.; Shangguan, W. Low-temperature catalysis for VOCs removal in technology and application: A state-of-the-art review. *Catal. Today* **2016**, *264*, 270−278.

(5) Nie, L.; Yu, J.; Jaroniec, M.; Tao, F. Room-temperature catalytic oxidation of formaldehyde on catalysts. *Catal. Sci. Technol.* **2016**, *6*, 3649−3669.

(6) Zhang, C.; Liu, F.; Zhai, Y.; Ariga, H.; Yi, N.; Liu, Y.; Asakura, K.; Flytzani-Stephanopoulos, M.; He, H. Alkali-metal-promoted Pt/TiO_2 opens a more efficient pathway to formaldehyde oxidation at ambient temperatures. *Angew. Chem., Int. Ed.* **2012**, *51*, 9628−9632.
(7) Sun, X.; Lin, J.; Guan, H.; Li, L.; Sun, L.; Wang, Y.; Miao, S.; Su, Y.; Wang, X. Complete oxidation of formaldehyde over TiO_2 supported subnanometer Rh catalyst at ambient temperature. *Appl. Catal., B* **2018**, *226*, 575−584.
(8) Wang, L.; Yue, H.; Hua, Z.; Wang, H.; Li, X.; Li, L. Highly active Pt/Na_xTiO_2 catalyst for low temperature formaldehyde decomposition. *Appl. Catal., B* **2017**, *219*, 301−313.
(9) Colussi, S.; Boaro, M.; De Rogatis, L.; Pappacena, A.; de Leitenburg, C.; Llorca, J.; Trovarelli, A. Room temperature oxidation of formaldehyde on Pt-based catalysts: A comparison between ceria and other supports (TiO_2, Al_2O_3 and ZrO_2). *Catal. Today* **2015**, *253*, 163−171.
(10) Li, L.; Wang, L.; Zhao, X.; Wei, T.; Wang, H.; Li, X.; Gu, X.; Yan, N.; Li, L.; Xiao, H. Excellent low-temperature formaldehyde decomposition performance over pt nanoparticles directly loaded on cellulose triacetate. *Ind. Eng. Chem. Res.* **2020**, *59*, 21720−21728.
(11) Wang, C.; Li, Y.; Zheng, L.; Zhang, C.; Wang, Y.; Shan, W.; Liu, F.; He, H. A nonoxide catalyst system study: alkali metal-promoted Pt/AC catalyst for formaldehyde oxidation at ambient temperature. *ACS Catal.* **2020**, *11*, 456−465.
(12) Huang, Y.; Long, B.; Tang, M.; Rui, Z.; Balogun, M.; Tong, Y.; Ji, H. Bifunctional catalytic material: an ultrastable and high-performance surface defect CeO_2 nanosheets for formaldehyde thermal oxidation and photocatalytic oxidation. *Appl. Catal., B* **2016**, *181*, 779−787.
(13) Zhu, S.; Zheng, J.; Xin, S.; Nie, L. Preparation of flexible Pt/TiO_2/γ-Al_2O_3 nanofiber paper for room-temperature HCHO oxidation and particulate filtration. *Chem. Eng. J.* **2022**, *427*, No. 130951.
(14) Zhang, L.; Chen, L.; Li, Y.; Peng, Y.; Chen, F.; Wang, L.; Zhang, C.; Meng, X.; He, H.; Xiao, F. Complete oxidation of formaldehyde at room temperature over an Al-rich Beta zeolite supported platinum catalyst. *Appl. Catal., B* **2017**, *219*, 200−208.
(15) Qi, L.; Cheng, B.; Yu, J.; Ho, W. High-surface area mesoporous Pt/TiO_2 hollow chains for efficient formaldehyde decomposition at ambient temperature. *J. Hazard. Mater.* **2016**, *301*, 522−530.
(16) Li, Y.; Zhang, C.; Ma, J.; Chen, M.; Deng, H.; He, H. High temperature reduction dramatically promotes Pd/TiO_2 catalyst for ambient formaldehyde oxidation. *Appl. Catal., B* **2017**, *217*, 560−569.
(17) Li, Y.; Zhang, C.; He, H.; Zhang, J.; Chen, M. Influence of alkali metals on Pd/TiO_2 catalysts for catalytic oxidation of formaldehyde at room temperature. *Catal. Sci. Technol.* **2016**, *6*, 2289−2295.
(18) Zhang, C.; He, H.; Tanaka, K. Perfect catalytic oxidation of formaldehyde over a Pt/TiO_2 catalyst at room temperature. *Catal. Commun.* **2005**, *6*, 211−214.
(19) Shi, K.; Wang, L.; Li, L.; Zhao, X.; Chen, Y.; Hua, Z.; Li, X.; Gu, X.; Li, L. Mild preoxidation treatment of Pt/TiO_2 catalyst and its enhanced low temperature formaldehyde decomposition. *Catalysts* **2019**, *9*, 694.
(20) Xu, F.; Le, Y.; Cheng, B.; Jiang, C. Effect of calcination temperature on formaldehyde oxidation performance of Pt/TiO_2 nanofiber composite at room temperature. *Appl. Surf. Sci.* **2017**, *426*, 333−341.
(21) Qi, L.; Ho, W.; Wang, J.; Zhang, P.; Yu, J. Enhanced catalytic activity of hierarchically macro−/mesoporous Pt/TiO_2 toward room-temperature decomposition of formaldehyde. *Catal. Sci. Technol.* **2015**, *5*, 2366−2377.
(22) Li, W.; Liu, C.; Zhou, Y.; Bai, Y.; Feng, X.; Yang, Z.; Lu, L.; Lu, X.; Chan, K. Enhanced photocatalytic activity in anatase/TiO_2(B) core−shell nanofiber. *J. Phys. Chem. C* **2008**, *112*, 20539−20545.
(23) Opra, D. P.; Gnedenkov, S. V.; Sinebryukhov, S. L. Recent efforts in design of TiO_2(B) anodes for high-rate lithium-ion batteries: A review. *J. Power Sources* **2019**, *442*, No. 227225.
(24) Yin, Z.; Wang, Z.; Wang, J.; Wang, X.; Song, T.; Wang, Z.; Ma, Y. HF promoted increased nitrogen doping in TiO_2(B) photocatalyst. *Chem. Commun.* **2020**, *56*, 5609−5612.
(25) Liu, W.; Wang, J.; Li, W.; Guo, X.; Lu, L.; Lu, X.; Feng, X.; Liu, C.; Yang, Z. A shortcut for evaluating activities of TiO_2 facets: water dissociative chemisorption on TiO_2-B (100) and (001). *Phys. Chem. Chem. Phys.* **2010**, *12*, 8721−8727.
(26) Li, L.; Yue, H.; Ji, T.; Li, W.; Zhao, X.; Wang, L.; She, J.; Gu, X.; Li, X. Novel mesoporous TiO_2(B) whisker-supported sulfated solid superacid with unique acid characteristics and catalytic performances. *Appl. Catal., A* **2019**, *574*, 25−32.
(27) Vittadini, A.; Casarin, M.; Selloni, A. Structure and stability of TiO_2-B surfaces: A density functional study. *J. Phys. Chem. C* **2009**, *113*, 18973−18977.
(28) Li, L.; Li, L.; Wang, L.; Zhao, X.; Hua, Z.; Chen, Y.; Li, X.; Gu, X. Enhanced catalytic decomposition of formaldehyde in low temperature and dry environment over silicate-decorated titania supported sodium-stabilized platinum catalyst. *Appl. Catal., B* **2020**, *277*, No. 119216.
(29) Yan, Z.; Xu, Z.; Yu, J.; Jaroniec, M. Enhanced formaldehyde oxidation on CeO_2/AlOOH-supported Pt catalyst at room temperature. *Appl. Catal., B* **2016**, *199*, 458−465.
(30) Huang, H.; Ye, X.; Huang, H.; Zhang, L.; Leung, D. Y. Mechanistic study on formaldehyde removal over Pd/TiO_2 catalysts: Oxygen transfer and role of water vapor. *Chem. Eng. J.* **2013**, *230*, 73−79.
(31) Kwon, D. W.; Seo, P. W.; Kim, G. J.; Hong, S. C. Characteristics of the HCHO oxidation reaction over Pt/TiO_2 catalysts at room temperature: the effect of relative humidity on catalytic activity. *Appl. Catal., B* **2015**, *163*, 436−443.
(32) Lin, L.; Kavadiya, S.; He, X.; Wang, W.; Karakocak, B.; Lin, Y.; Berezin, M. Y.; Biswas, P. Engineering stable Pt nanoparticles and oxygen vacancies on defective TiO_2 via introducing strong electronic metal-support interaction for efficient CO_2 photoreduction. *Chem. Eng. J.* **2020**, *389*, No. 123450.
(33) Beuvier, T.; Richard-Plouet, M.; Brohan, L. Accurate Methods for Quantifying the Relative Ratio of Anatase and TiO_2(B) Nanoparticles. *J. Phys. Chem. C* **2009**, *113*, 13703−13706.
(34) Thommes, M.; Kaneko, K.; Neimark, A. V.; Olivier, J. P.; Rodriguez-Reinoso, F.; Rouquerol, J.; Sing, K. S. Physisorption of gases, with special reference to the evaluation of surface area and pore size distribution (IUPAC Technical Report). *Pure Appl. Chem.* **2015**, *87*, 1051−1069.
(35) Chen, H.; Rui, Z.; Ji, H. Monolith-like TiO_2 nanotube array supported Pt catalyst for HCHO removal under mild conditions. *Ind. Eng. Chem. Res.* **2014**, *53*, 7629−7636.
(36) Chen, H.; Rui, Z.; Ji, H. Titania-supported Pt catalyst reduced with HCHO for HCHO oxidation under mild conditions. *Chin. J. Catal.* **2015**, *36*, 188−196.
(37) Zhang, C.; He, H.; Tanaka, K. Catalytic performance and mechanism of a Pt/TiO_2 catalyst for the oxidation of formaldehyde at room temperature. *Appl. Catal., B* **2006**, *65*, 37−43.
(38) Cui, W.; Wang, X.; Tan, N. Effect of thermal treatment temperature on catalytic performance of Pt/TiO_2 nanobelt composite for HCHO oxidation. *J. Fuel Chem. Technol.* **2021**, *49*, 1701−1708.
(39) Chen, X.; Wang, H.; Chen, M.; Qin, X.; He, H.; Zhang, C. Co-function mechanism of multiple active sites over Ag/TiO_2 for formaldehyde oxidation. *Appl. Catal., B* **2021**, *282*, No. 119543.
(40) Chen, H.; Rui, Z.; Wang, X.; Ji, H. Multifunctional Pt/ZSM-5 catalyst for complete oxidation of gaseous formaldehyde at ambient temperature. *Catal. Today* **2015**, *258*, 56−63.
(41) An, N.; Yu, Q.; Liu, G.; Li, S.; Jia, M.; Zhang, W. Complete oxidation of formaldehyde at ambient temperature over supported Pt/Fe_2O_3 catalysts prepared by colloid-deposition method. *J. Hazard. Mater.* **2011**, *186*, 1392−1397.
(42) Qu, Z.; Shen, S.; Chen, D.; Wang, Y. Highly active Ag/SBA-15 catalyst using post-grafting method for formaldehyde oxidation. *J. Mol. Catal. A: Chem.* **2012**, *356*, 171−177.

https://doi.org/10.1021/acsomega.2c02490
ACS Omega 2022, 7, 25491−25501

(43) Li, H.; Liu, X.; Guo, C.; Liu, T.; Luo, M.; Lu, J. Support effect on catalytic oxidation of formaldehyde over supported gold catalysts. *Chin. J. Catal.* **2009**, *30*, 1001.
(44) Ma, C.; Wang, D.; Xue, W.; Dou, B.; Wang, H.; Hao, Z. Investigation of formaldehyde oxidation over $Co_3O4-CeO_2$ and $Au/Co_3O_4-CeO_2$ catalysts at room temperature: effective removal and determination of reaction mechanism. *Environ. Sci. Technol.* **2011**, *45*, 3628−3634.
(45) Dong, Y.; Zhang, G.; Wang, M.; Li, N.; Xu, Q.; Li, H.; He, J.; Lu, J. Pt/MnO_2 Nanoflowers Anchored to Boron Nitride Aerogels for Highly Efficient Enrichment and Catalytic Oxidation of Formaldehyde at Room Temperature. *Angew. Chem.* **2021**, *133*, 6447−6451.
(46) Duan, Y.; Song, S.; Cheng, B.; Yu, J.; Jiang, C. Effects of hierarchical structure on the performance of tin oxide-supported platinum catalyst for room-temperature formaldehyde oxidation. *Chin. J. Catal.* **2017**, *38*, 199−206.
(47) Su, Y.; Ji, K.; Xun, J.; Zhang, K.; Liu, P.; Zhao, L. Catalytic oxidation of low concentration formaldehyde over Pt/TiO_2 catalyst. *Chin. J. Chem. Eng.* **2021**, *29*, 190−195.
(48) Ruiz-Martínez, J.; Sepúlveda-Escribano, A.; Anderson, J. A.; Rodríguez-Reinoso, F. Spectroscopic and microcalorimetric study of a TiO_2-supported platinum catalyst. *Phys. Chem. Chem. Phys.* **2009**, *11*, 917−920.
(49) Lane, G. S.; Wolf, E. E. Characterization and Fourier transform infrared studies of the effects of TiO_2 crystal phases during CO oxidation on Pt/TiO_2 catalysts. *J. Catal.* **1987**, *105*, 386−404.
(50) Lin, M.; Yu, X.; Yang, X.; Li, K.; Ge, M.; Li, J. Highly active and stable interface derived from Pt supported on Ni/Fe layered double oxides for HCHO oxidation. *Catal. Sci. Technol.* **2017**, *7*, 1573−1580.
(51) Kale, M. J.; Christopher, P. Utilizing quantitative in situ FTIR spectroscopy to identify well-coordinated Pt atoms as the active site for CO oxidation on Al_2O_3-supported Pt catalysts. *ACS Catal.* **2016**, *6*, 5599−5609.
(52) Chen, C.; Chen, F.; Zhang, L.; Pan, S.; Bian, C.; Zheng, X.; Meng, X.; Xiao, F. Importance of platinum particle size for complete oxidation of toluene over Pt/ZSM-5 catalysts. *Chem. Commun.* **2015**, *51*, 5936−5938.
(53) Wang, C.; Li, Y.; Zhang, C.; Chen, X.; Liu, C.; Weng, W.; Shan, W.; He, H. A simple strategy to improve Pd dispersion and enhance Pd/TiO_2 catalytic activity for formaldehyde oxidation: The roles of surface defects. *Appl. Catal., B* **2021**, *282*, No. 119540.
(54) Vovk, E. I.; Kalinkin, A. V.; Smirnov, M. Y.; Klembovskii, I. O.; Bukhtiyarov, V. I. XPS study of stability and reactivity of oxidized Pt nanoparticles supported on TiO_2. *J. Phys. Chem. C* **2017**, *121*, 17297−17304.
(55) Fiala, R.; Figueroba, A.; Bruix, A.; Vaclavu, M.; Rednyk, A.; Khalakhan, I.; Vorokhta, M.; Lavkova, J.; Illas, F.; Potin, V. High efficiency of Pt^{2+}-CeO_2 novel thin film catalyst as anode for proton exchange membrane fuel cells. *Appl. Catal., B* **2016**, *197*, 262−270.
(56) Zhang, L.; Cheng, X.; Zhang, G.; Qiu, W.; He, H.; Chen, G. High active platinum clusters on titanium dioxide supports toward carbon monoxide oxidation. *Appl. Catal., B* **2020**, *266*, No. 118629.
(57) Xu, Z. H.; Huang, G.; Yan, Z. X.; Wang, N. H.; Yue, L.; Liu, Q. Y. Hydroxyapatite-Supported Low-Content Pt Catalysts for Efficient Removal of Formaldehyde at Room Temperature. *ACS Omega* **2019**, *4*, 21998−22007.
(58) He, M.; Ji, J.; Liu, B.; Huang, H. Reduced TiO_2 with tunable oxygen vacancies for catalytic oxidation of formaldehyde at room temperature. *Appl. Surf. Sci.* **2019**, *473*, 934−942.
(59) Chen, H.; Tang, M.; Rui, Z.; Ji, H. MnO_2 promoted TiO_2 nanotube array supported Pt catalyst for formaldehyde oxidation with enhanced efficiency. *Ind. Eng. Chem. Res.* **2015**, *54*, 8900−8907.
(60) Chen, J.; Ding, J.; Li, H.; Sun, J.; Rui, Z.; Ji, H. Pt supported on long-rod β-FeOOH as an efficient catalyst for HCHO oxidation at ambient temperature. *Catal. Sci. Technol.* **2019**, *9*, 3287−3294.
(61) Liu, L.; McAllister, B.; Ye, H.; Hu, P. Identifying an O_2 supply pathway in CO oxidation on Au/TiO_2 (110): A density functional theory study on the intrinsic role of water. *J. Am. Chem. Soc.* **2006**, *128*, 4017−4022.
(62) Yan, Z.; Xu, Z.; Yu, J.; Jaroniec, M. Highly Active Mesoporous Ferrihydrite Supported Pt Catalyst for Formaldehyde Removal at Room Temperature. *Environ. Sci. Technol.* **2015**, *49*, 6637−6644.
(63) Yan, Z.; Xu, Z.; Yu, J.; Jaroniec, M. Effect of microstructure and surface hydroxyls on the catalytic activity of Au/AlOOH for formaldehyde removal at room temperature. *J. Colloid Interface Sci.* **2017**, *501*, 164−174.
(64) Wu, H.; Chen, T.; Chen, Y.; Lee, J. F.; Chen, C. Formaldehyde oxidation on silica-supported Pt catalysts: the influence of thermal pretreatments on particle formation and on oxidation mechanism. *J. Catal.* **2017**, *355*, 87−100.
(65) Huang, Y.; Xu, H.; Yang, H.; Lin, Y.; Liu, H.; Tong, Y. Efficient Charges Separation Using Advanced BiOI-Based Hollow Spheres Decorated with Palladium and Manganese Dioxide Nanoparticles. *ACS Sustainable Chem. Eng.* **2018**, *6*, 2751−2757.
(66) Chen, X.; He, G.; Li, Y.; Chen, M.; Qin, X.; Zhang, C.; He, H. Identification of a facile pathway for dioxymethylene conversion to formate catalyzed by surface hydroxyl on TiO_2-based catalyst. *ACS Catal.* **2020**, *10*, 9706−9715.
(67) Zhang, L.; Bao, Q.; Zhang, B.; Zhang, Y.; Wan, S.; Wang, S.; Lin, J.; Xiong, H.; Mei, D.; Wang, Y. Distinct Role of Surface Hydroxyls in Single-Atom $Pt1/CeO_2$ Catalyst for Room-Temperature Formaldehyde Oxidation: Acid−Base Versus Redox. *JACS Au.* **2022**, DOI: 10.1021/jacsau.2c00215.
(68) Finnie, K. S.; Cassidy, D. J.; Bartlett, J. R.; Woolfrey, J. L. IR spectroscopy of surface water and hydroxyl species on nanocrystalline TiO_2 films. *Langmuir* **2001**, *17*, 816−820.
(69) Wang, J.; Zhang, P.; Li, J.; Jiang, C.; Yunus, R.; Kim, J. Room-temperature oxidation of formaldehyde by layered manganese oxide: effect of water. *Environ. Sci. Technol.* **2015**, *49*, 12372−12379.
(70) Tsyganenko, A.; Filimonov, V. Infrared spectra of surface hydroxyl groups and crystalline structure of oxides. *Spectrosc. Lett.* **1972**, *5*, 477−487.
(71) Liu, H.; Liew, K.; Pan, C. Influence of hydroxyl groups on the adsorption of HCHO on TiO_2-B (100) surface by first-principles study. *Phys. Chem. Chem. Phys.* **2013**, *15*, 3866−3880.
(72) Fang, W.; Liu, W.; Guo, X.; Lu, X.; Lu, L. Theoretical investigation of CO adsorption on clean and hydroxylated TiO_2-B (100) surfaces. *J. Phys. Chem. C* **2011**, *115*, 8622−8629.
(73) Zhuang, W.; Lu, L.; Wu, X.; Jin, W.; Meng, M.; Zhu, Y.; Lu, X. TiO_2-B nanofibers with high thermal stability as improved anodes for lithium ion batteries. *Electrochem. Commun.* **2013**, *27*, 124−127.

https://doi.org/10.1021/acsomega.2c02490
ACS Omega 2022, 7, 25491−25501